catalysts

MDPI

Article

Investigations on Structural, Electronic and Optical Properties of MoS_2/CDs Heterostructure via First-Principles Study

Xianglu Yin [1,*,†], Aijun Teng [1,*,†], Zhi Chang [2], Peng Yuan [3], Dongbin Zhang [1] and Jiyang Yu [1]

[1] Ansteel Beijing Research Institute Co., Ltd., Beijing 102209, China; zhangdongbin@ansteel.com.cn (D.Z.); yujiyang@ansteel.com.cn (J.Y.)
[2] Pangang Group Vanadium Titanium & Resources Co., Ltd., Panzhihua 617067, China; changz1221_80@126.com
[3] School of Chemical Engineering & Technology, Hebei University of Technology, Tianjin 300401, China; yuanpeng@hebut.edu.cn
* Correspondence: yinxianglu@ansteel.com.cn (X.Y.); tengaijun@ansteel.com.cn (A.T.)
† These authors contributed equally to this work.

Abstract: Much effort has been made for MoS_2/CDs heterostructure application in the field of photocatalysts. However, the impacts of functional groups of CDs on the properties of the heterostructure are ambiguous. Here, the impacts of hydroxyl, carbonyl, and carboxyl groups of CDs on the structural, electronic, and optical properties of MoS_2/CDs' heterostructure were investigated by conducting a first-principles study. The calculated energy band structure and band gap of monolayer MoS_2 were consistent with the experimental values. The band gap of MoS_2 was obviously decreased after the construction of MoS_2/CDs and MoS_2/CDs–hydroxyl/carboxyl, thus helping to improve the light adsorption range. However, the band gap of MoS_2/CDs–carbonyl was slightly increased compared with that of monolayer MoS_2. The CDs with functional groups can spontaneously bind on 2D-MoS_2 and form a stable MoS_2/CDs heterostructure. It was confirmed that the MoS_2/CDs' heterostructure belongs to the typical type-II band alignment, which contributes to the separation of photogenerated charge and hole. Notably, the carbonyl and carboxyl groups on the CDs obviously reduced the optical absorption intensity of the MoS_2/CDs in the ultraviolet region. The hydroxyl groups have little effect on optical absorption intensity. Thus, the CDs with more hydroxyl groups are beneficial to produce a higher photocatalytic performance. This paper reveals the impacts of surface functional groups and provides a promising approach for designing the MoS_2/CDs' heterostructure to enhance the photocatalytic properties.

Keywords: MoS_2/CDs heterostructure; first-principles study; type-II band alignment; photocatalytic

check for updates

Citation: Yin, X.; Teng, A.; Chang, Z.; Yuan, P.; Zhang, D.; Yu, J. Investigations on Structural, Electronic and Optical Properties of MoS_2/CDs Heterostructure via First-Principles Study. *Catalysts* **2022**, *12*, 456. https://doi.org/10.3390/catal12050456

Academic Editor: Bruno Fabre

Received: 11 March 2022
Accepted: 15 April 2022
Published: 20 April 2022

1. Introduction

Molybdenum disulfide (MoS_2) is one of the most studied novel material among transition metal sulfides, due to its potential applications in electronic and optoelectronic devices [1–3], hydrogen evolution reaction [4–6], and energy storage [7–9]. However, MoS_2 also has some disadvantages in practical applications, including the inert basal plane, untunable band gap, and low conductivity [10,11]. Therefore, in order to activate the basal plane, enhance conductivity, and tune band-gap, MoS_2-based heterostructures and hybrid systems have been built. The MoS_2-based heterostructures include carbon materials (graphene, graphene oxide, graphene quantum dot, carbon dot, and carbon nanotube), noble metals (Ag, Au, and Pt), TiO_2, Cu_2O, MoO_3, and other two-dimensional materials (WS_2, WSe, BN, and Mxenes) [12–21], exhibiting the better performance in terms of electronics, optoelectronics, catalytics, and energy storage.

Carbon materials play a key role in these MoS_2-based heterostructures, due to their unique electronic properties. However, some unexpected functional groups always are produced from the preparation of carbon materials such as graphene, graphene oxide,

and carbon dot. The impacts of functional groups on MoS_2-based heterostructures are vague. In this paper, we chose carbon dots (CDs) as a representative carbon material for researching the impacts of functional groups on the electronic properties. Carbon dots are a common carbon material, because they have extensive applications in photocatalysis [22], bio-imaging [23], sensor [24], and light-emitting diodes [25], due to high quantum yields and tunable light-emission bands. Chen et al. [26] prepared 1L-MoS_2/CDs ultra-thin light emission films with full-color tunable photoluminescence, which greatly extended the light emission bands of MoS_2. Badhulika et al. [16] first fabricated a 2D-MoS_2-CDs-based flexible broadband photodetector covering the entire range of the electromagnetic spectrum, due to the combination of UV illumination of CDs and visible and NIR illumination of MoS_2. To date, the facile and green preparation of CDs is the carbonization of carbon sources, including glucose [27], citric acid [26], sugar [28], and chia seed [16]. Many experiments have demonstrated that the hydroxyl, carbonyl, and carboxyl groups exist in the edge of CDs due to the incomplete carbonization [27,29]. It is well-known that the surface functional groups have a strong influence on electronic structures, optical characteristics, and conductivity [26,30–33]. However, due to the difficulty of synthesizing CDs with a specific functional group, the influence of a specific functional group is hard to study through experimentation. Therefore, it is of great significance to study it through simulation calculations.

Density functional theory (DFT) calculation is a powerful and scientific technology that is used to research the intrinsic properties of nanomaterials and provide theoretical guidance for experiments and applications. Some papers have reported the effects of vacancies or heterostructure on the structural, electronic, and optical properties of monolayer MoS_2 by DFT [30,31]. However, the influences of the surface properties of CDs on the properties of MoS_2/CDs were less investigated through simulation. In this study, the effects of hydroxyl, carbonyl, and carboxyl groups of CDs on the structural, electronic, and optical properties of MoS_2/CDs' heterostructure were revealed by applying density functional theory. This study contributes to improving the optical property of MoS_2/CDs' heterostructure.

2. Computational Details

All the first-principles calculations were performed within the framework of the plane-wave pseudopotential density functional theory (DFT) implemented in CASTEP code with ultrasoft pseudopotential method on the basis of DFT [34–36]. The generalized gradient approximation (GGA) with Perdew–Bruke–Ernzerhof (PBE) functional and van der Waals correction proposed by the Grimme potential were employed [34,37]. This method has widely been employed to study the structural, electronic, and photoelectronic properties of MoS_2-based heterostructure [34,38–40]. All structures were relaxed until the force on each atom was less than 0.01 eV $Å^{-1}$. The energy cutoff was 400 eV. The two-dimensional (2D) periodic boundary conditions were considered along the growth directions of the MoS_2/CDs layer. The Monkhorst–Pack k-point mesh was sampled with a separation of 0.05 and 0.015 $Å^{-1}$ in the Brillouin zone during the relaxation and calculation periods, respectively.

3. Results and Discussions

First, a 4 × 4 supercell of MoS_2 monolayer composed of 16 molybdenum atoms and 32 sulfur atoms was constructed as a substrate (Figure 1a). A zigzag-edged $C_{24}H_{12}$ structure was used, and all edge carbon atoms of CDs were assumed to be fully passivated by H atoms to eliminate the dangling bonds (Figure 1b) [34,41]. It has been widely accepted that the carboxyl, hydroxyl, and carbonyl are three dominant functional groups on the CDs. Therefore, the CDs-T (T is carboxyl, hydroxyl, and carbonyl, respectively; CDs-T represents that only one functional group T is on the CDs) were constructed for studying the impacts of functional groups on the structure, electronic, and optical absorption of MoS_2/CDs. In order to match the experimental data, the functional groups were place on the edge of CDs. After geometry optimization, the lattice constants of the MoS_2 monolayer

were a = b = 3.191 Å and $\alpha = \beta = 90°$, $\gamma = 120°$, which is comparable to the experimentally measure for the bulk MoS_2 [42]. To evaluate the structural stability of MoS_2/CDs-T, the binding energies were calculated by using the Equation (1) [39].

$$E_b = E_{(MoS2/CDs\text{-}T)} - E_{(MoS2)} - E_{(CDs\text{-}T)} \quad (1)$$

where $E_{(MoS2/CDs\text{-}T)}$, $E_{(MoS2)}$, and $E_{(CDs\text{-}T)}$ are the total energies of MoS_2/CDs-T, MoS_2, and CDs-T, respectively.

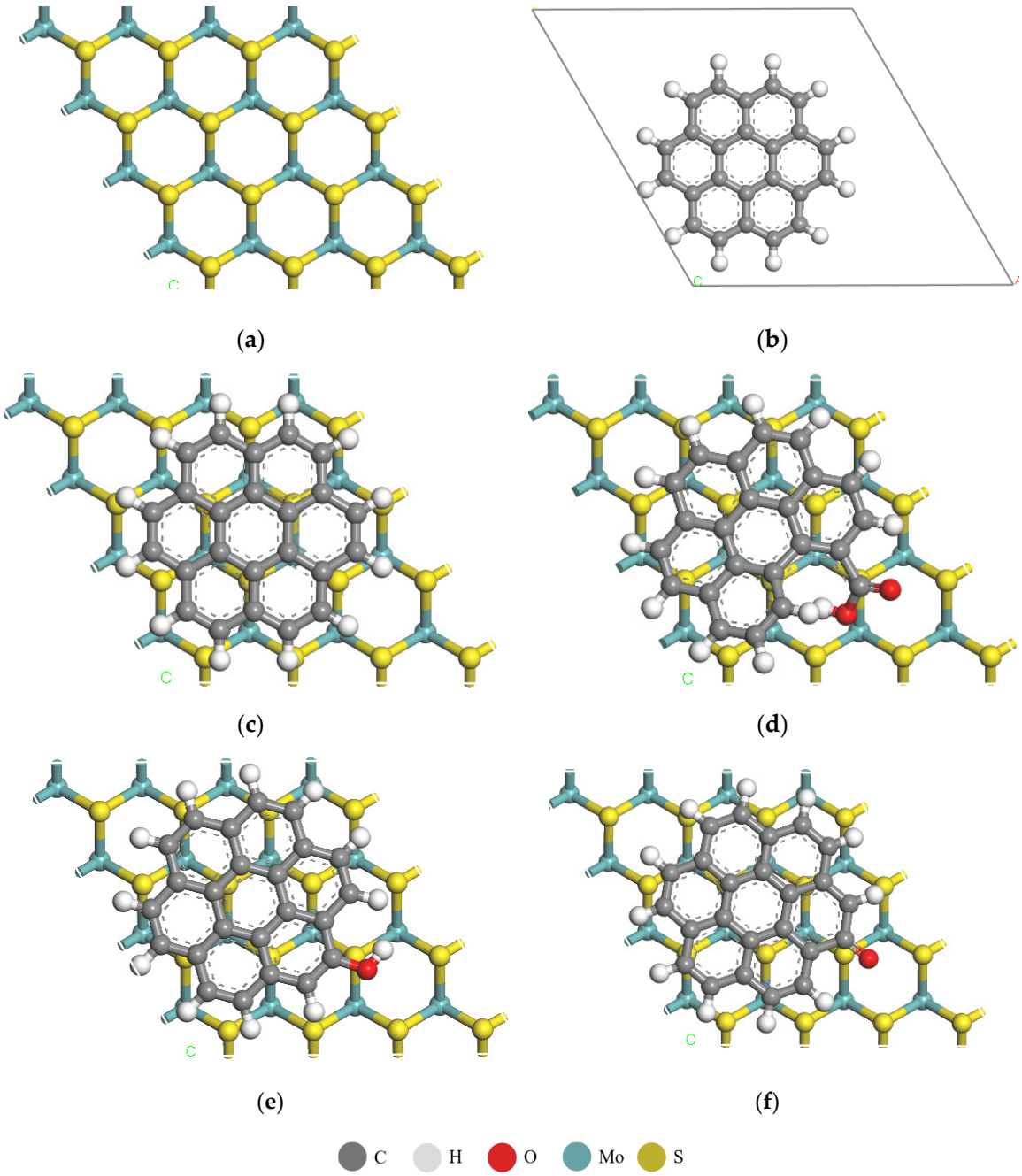

Figure 1. Geometrical structures of MoS_2 monolayer (**a**), CDs (**b**), MoS_2/CDs heterostructures without groups (**c**), MoS_2/CDs heterostructures with carboxyl (**d**), hydroxyl (**e**), and carbonyl (**f**).

Figure 2a shows the E_b and h (the distance between MoS_2 and CDs and CDs-T) in the heterostructures. The optimized h value ranges from 3.267 to 3.358 Å, and the closest

distance is 3.267 Å of MoS_2/CDs-OH. The bigger carboxyl groups on the CDs increase the distance due to the steric effect. The negative binding energy suggests that CDs spontaneously form the MoS_2/CDs' heterostructure and keep it in a stable state. A negative binding energy indicates that the two substances can spontaneously bind and form a stable heterojunction. Conversely, a positive binding energy indicates that the two substances cannot bind spontaneously. Therefore, the carboxyl, hydroxyl, and carbonyl groups on the CDs can still form the stability of the MoS_2/CDs-T heterostructures. Figure 2b,c shows the band structure and partial density of the MoS_2 states. The direct band gap (the conduction band minimum and the valence band maximum are located at the K symmetry point indicating) of 1.75 eV (Figure 2b) for monolayer MoS_2 is in good agreement with other theoretical values (1.78 eV [43], 1.74 eV [34], and 1.70 eV [43]) and experimental results (1.75 eV [44] and 1.80 eV [45]). As shown in Figure 2c, the valence bands and the conduction bands are essentially hybridized from the Mo 4d and S 3p orbitals, and this is in accordance with the previous calculation results [34,46].

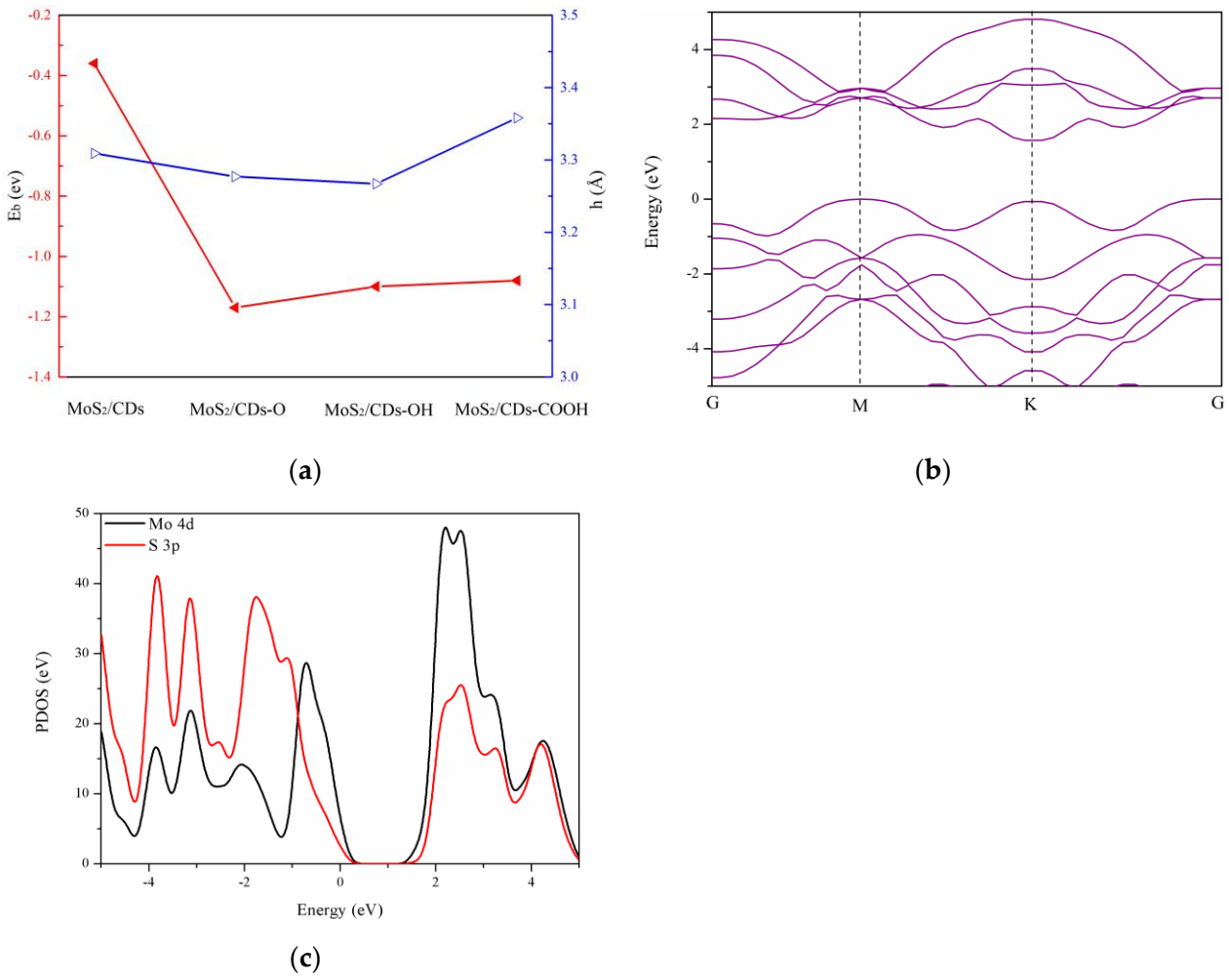

Figure 2. The binding energy (E_b) and distance (h) of MoS_2/CDs-T (**a**), band structure of MoS_2 monolayer (**b**), and partial density of states (PDOS) of MoS_2 monolayer (**c**).

Figure 3 displays the PDOS of CDs and CDs-T; the insets in these figures are the corresponding band structures. Electron transfer and sharing between functional groups and carbon atoms lead to changes in the electronic structure. The valence bands of CDs from −5 to −2 eV are mainly hybridized from C 2p and H 1s orbitals, while the valence bands from −2 to 0 eV and the conduction bands from 0 to 4 eV are composed only of C 2p orbital (Figure 3a). Moreover, the energy levels of CDs are discrete, owing to the

quantum confinement [34]. The energy gap of CDs between the highest occupied molecular orbital (HOMO) and the lowest unoccupied molecular orbital (LUMO) is 2.859 eV, which is really agreement with previously reported results (2.890 eV [34] and 2.90 eV [41]). It is worth noting that the energy gaps calculated by DFT are lower than the experimental result (5.56 eV [47] and 6.82 eV [48]), which results from the most used local and semi-local approximations for exchange–correlation functional in standard DFT calculation liable to underestimate energy gaps [46]. After hydroxyl, carbonyl, and carboxyl were added to CDs, the energy gaps of CDs-T between LUMO and HOMO were 2.637, 2.236, and 2.110 eV, respectively. As seen in Figure 3b–d, the valence bands of CDs-T from −5 to −2 eV and the conduction bands from 3.5 to 5 eV are hybridized from C 2p, O 2p, and H 1s orbitals, while the valence bands from −2 to 0 eV and the conduction bands from 0 to 3.5 eV are hybridized from major C 2p and a small part portion of O 2p orbitals. The bottom of the conduction bands and top of the valence bands of MoS_2/CDs-T consist of the hybridization from the C 2p and O 2p orbitals.

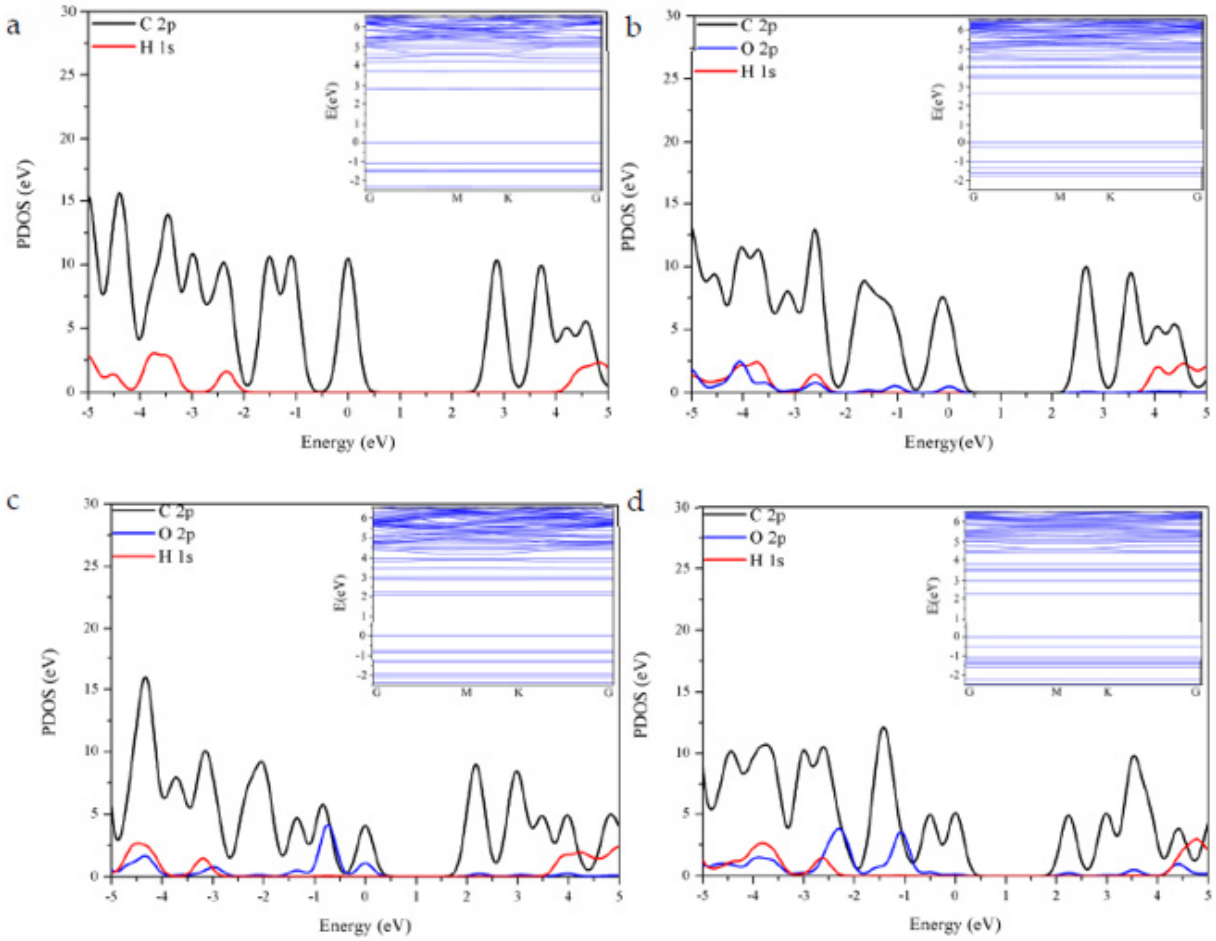

Figure 3. Partial density of states (PDOS) of pure CDs (**a**), CDs-T (T is hydroxyl (**b**), carbonyl (**c**), and carboxyl (**d**)); the insets in these figures are the corresponding band structures.

The PDOS and band structure of MoS_2/CDs and MoS_2/CDs-T heterostructures are shown in Figure 4. In the LUMO, the conduction bands of these heterostructures are mainly hybridized from Mo 4d and S 3p orbitals. There are energy levels under the Femi level. For MoS_2/CDs, MoS_2/CDs-OH, and COOH, these energy levels are mainly composed of the C 2p orbital. However, the energy level at the Femi level of MoS_2/CDs-O is hybridized from the C 2p and O 2p orbitals. The electronic structure indicates that the Mo 4d, S 3p, C 2p, and O 2p orbitals are the main way of photo-induced electron. Under the illumination, the electrons are transferred from CDs to MoS_2 and leave holes on the CDs, which contribute to

the separation of electron and hole. The energy bands of MoS_2/CDs, MoS_2/CDs–hydroxyl, and carboxyl are reduced to 1.496, 1.320, and 1.248 eV, respectively, while the energy band in MoS_2/CDs–carbonyl is 1.772 eV.

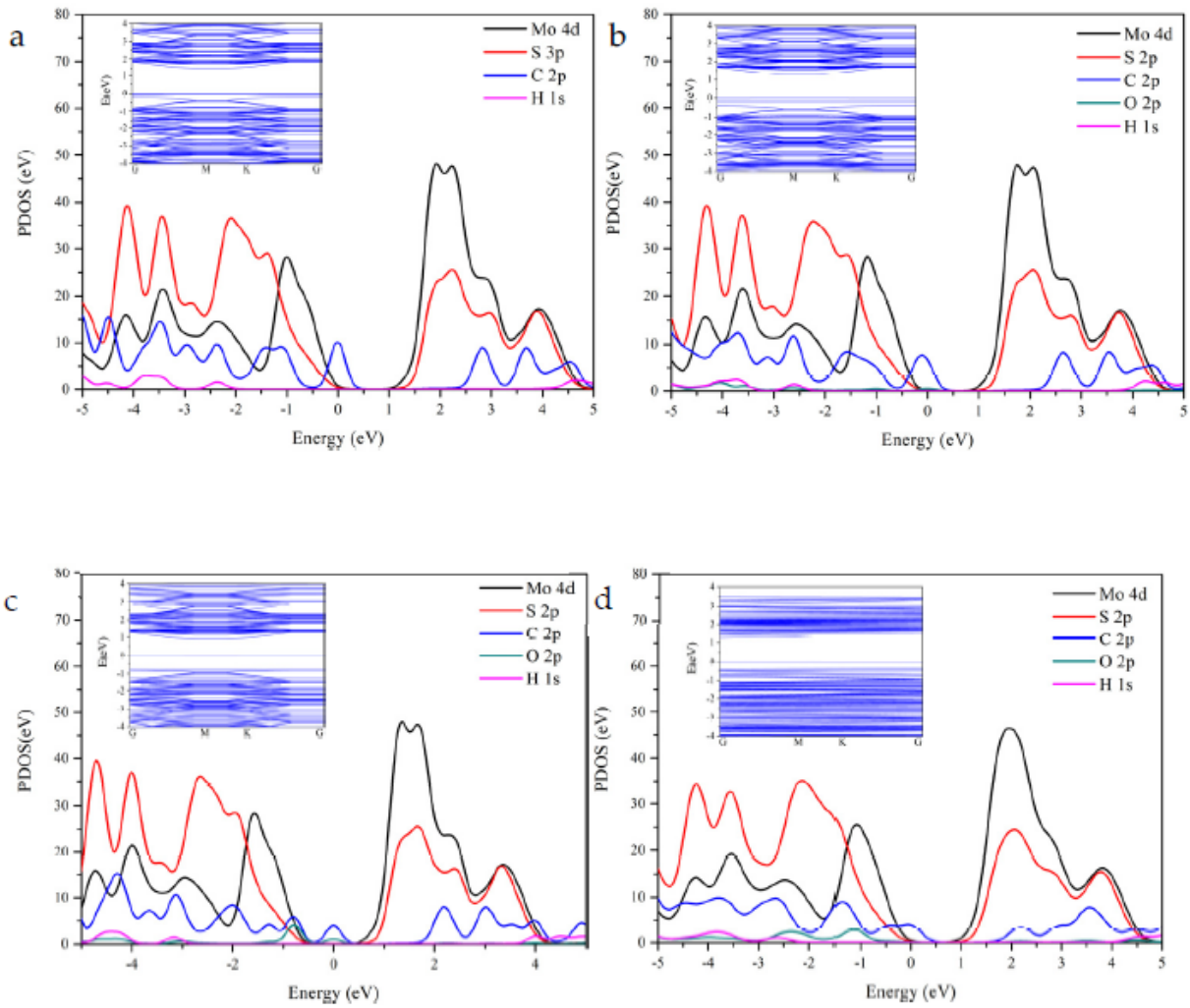

Figure 4. Partial density of states (PDOS) of MoS_2/CDs heterostructure (**a**), MoS_2/CDs-T heterostructures (T is hydroxyl (**b**), carbonyl (**c**), and carboxyl (**d**)); the insets in these figures are the corresponding band structures.

The optical absorption of the catalyst plays a key role in the photocatalytic process. Figure 5a shows the optical absorption spectra of these samples, namely CDs-T, MoS_2, and MoS_2/CDs-T. The frequency-dependent dielectric matrix, $\varepsilon(\omega) = \varepsilon_1(\omega) + i\varepsilon_2(\omega)$, is calculated, where $\varepsilon_1(\omega)$ and $\varepsilon_2(\omega)$ are the real and imaginary parts of the dielectric function, respectively. The $\varepsilon_1(\omega)$ is determined by summation over electronic states, using the Equation (2). [49]:

$$\varepsilon_1(\omega) = 1 + \frac{2}{\pi} P \int_0^{\infty} \frac{\varepsilon_2(\omega')\omega'}{\omega'^2 - \omega^2 + i\eta} d\omega' \quad (2)$$

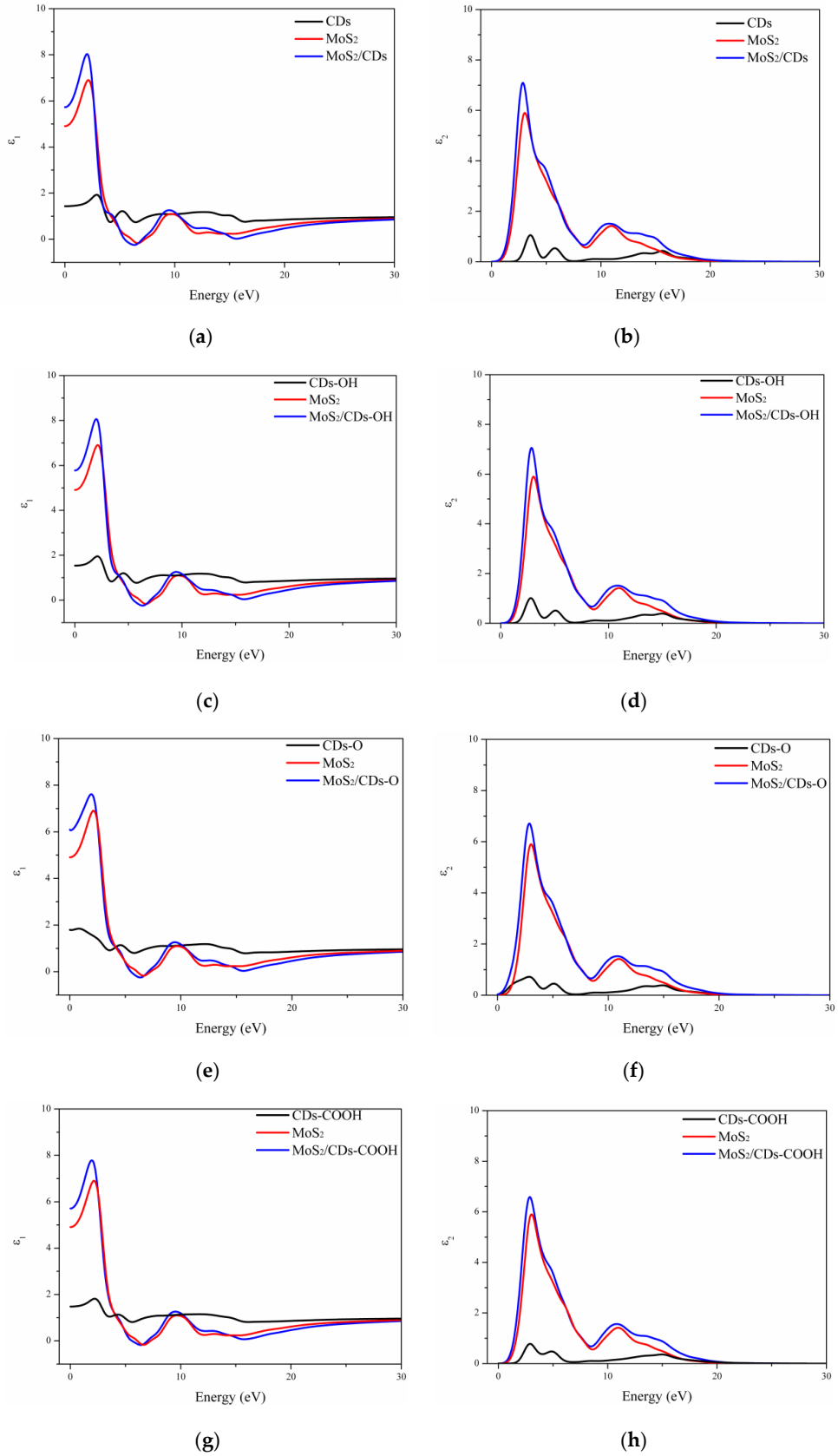

Figure 5. Real parts, ε_1 (ω) of (**a**) MoS_2/CDs, (**c**) MoS_2/CDs-OH, (**e**) MoS_2/CDs-OH, and (**g**) MoS_2/CDs-COOH. Imaginary parts, ε_2 (ω) of (**b**) MoS_2/CDs, (**d**) MoS_2/CDs-OH, (**f**) MoS_2/CDs-OH, and (**h**) MoS_2/CDs-COOH. Imaginary parts.

The $\varepsilon_2(\omega)$ is obtained by using the Kramers–Kronig relationship [45]:

$$\varepsilon_2(\omega) = \frac{4\pi^2 e^2}{\Omega} \lim_{q \to 0} \frac{1}{q^2} \sum_{c,v,\,k} 2\omega_k \delta(\varepsilon_{ck} - \varepsilon_{vk} - \omega) \times \langle \mu_{ck+e_\alpha q} | \mu_{vk} \rangle \langle \mu_{vk+e_\beta q} | \mu_{vk} \rangle \quad (3)$$

The light adsorption intensity is evaluated according to the Equation (4). [45]:

$$\alpha(\mathrm{E}) = \frac{4\pi e}{hc} \left\{ \frac{\left[\varepsilon_1^2 + \varepsilon_2^2\right]^{1/2} - \varepsilon_1}{2} \right\}^{1/2} \quad (4)$$

The calculated $\varepsilon_1(\omega)$ and $\varepsilon_2(\omega)$ of dielectric function versus energy of MoS_2, CDs-T, and MoS_2/CDs-T are shown in Figure 5. The peak A (3.01 eV), B(4.96 eV), and C(10.94 eV) can be observed in the imaginary part of MoS_2. These peaks are located from 0 to 30 eV, due to the absorptive transition from the valence bands to the conduction bands. According to the structure analysis, the peaks of A, B, and C result from the transition of S 3p into Mo 4d conduction bands [50], the hybridization orbitals between S 3p and Mo 4d into Mo 4d conduction bands [51], and σ bonding between S 3p and Mo 5s into Mo 4d conduction bands [52], respectively. For MoS_2/CDs-T, they have similar profiles with that of MoS_2. Notably, the imaginary parts of MoS_2/CDs-T move slightly toward lower energies because of the effects of heterostructure [53]. The calculated static constants of MoS_2 is about 5.0 eV, which is consistent with other reported values of 5.3 eV calculated by the generalized gradient approximation (GGA) with Perdew–Bruke–Ernzerhof functional [54]. It is obvious that the static dielectric constants of MoS_2/CDs-T are bigger than those of of MoS_2. Figure 6a shows the optical absorption spectra of all samples. There is strong absorption in the range of 200 to 700 nm for the MoS_2 monolayer, which is potential for applications in sunlight-driven photocatalysis. The main peak at about 450 nm is attributed to the transition from the occupied Mo-4d orbital to the unoccupied S-3p orbital [55]. However, the MoS_2 monolayer has a low adsorption capacity at the long wavelength end, and this results from the electronic structure of the monolayer. The absorption peaks of CDs are mainly located at the ultraviolet region from 200 to 400 nm, and the absorption intensity is relatively low. The obvious red shifts of the absorption peaks and the reduction of the absorption intensities can be observed after the MoS_2/CDs' heterostructures were constructed. Compared to the MoS_2 monolayer, the absorption intensities ranging from 200 nm to the long wavelength were obviously increased by CDs. However, the carbonyl and carboxyl groups of CDs decrease the absorption intensities of MoS_2/CDs in the ultraviolet region. In contrast, the hydroxyl groups have a slight impact on the absorption. It can be concluded that CDs are suitable for promoting the photocatalysis of MoS_2 due to the enhanced adsorption intensity. However, the carbonyl and carboxyl groups have a negative effect on the photocatalysis of MoS_2/CDs, causing a decrease in adsorption intensity.

To investigate the redox ability of MoS_2/CDs-T, the valence band maximum (VBM) and conduction band minimum (CBM) relative to the vacuum energy level were calculated according to the Equations (5) and (6). [55]:

$$\mathrm{E_{VB}} = \varphi = \mathrm{V}(\infty) - \mathrm{E_F} \quad (5)$$

$$\mathrm{E_{CB}} = \mathrm{E_{VB}} - \mathrm{E_g} \quad (6)$$

where V (∞), E_F, and E_g are the electrostatic potential in a vacuum region, the Fermi level of the neutral surface system, and the band gap, respectively. As shown in Figure 6b, the LUMO and HOMO of CDs-T are placed at higher energy states than the CBM and VBM of MoS_2 monolayer, respectively. It indicated that MoS_2/CDs heterostructures can construct the typical type-II band alignments [34], which promote photo-induced charge separation and transfer. Combining with the results from PDOS and band structures (Figure 4), the photo-generated electron of C 2p orbitals of CDs and CDs-T will transfer to the S 3p and Mo 4d hybrid orbitals (Figure 6c).

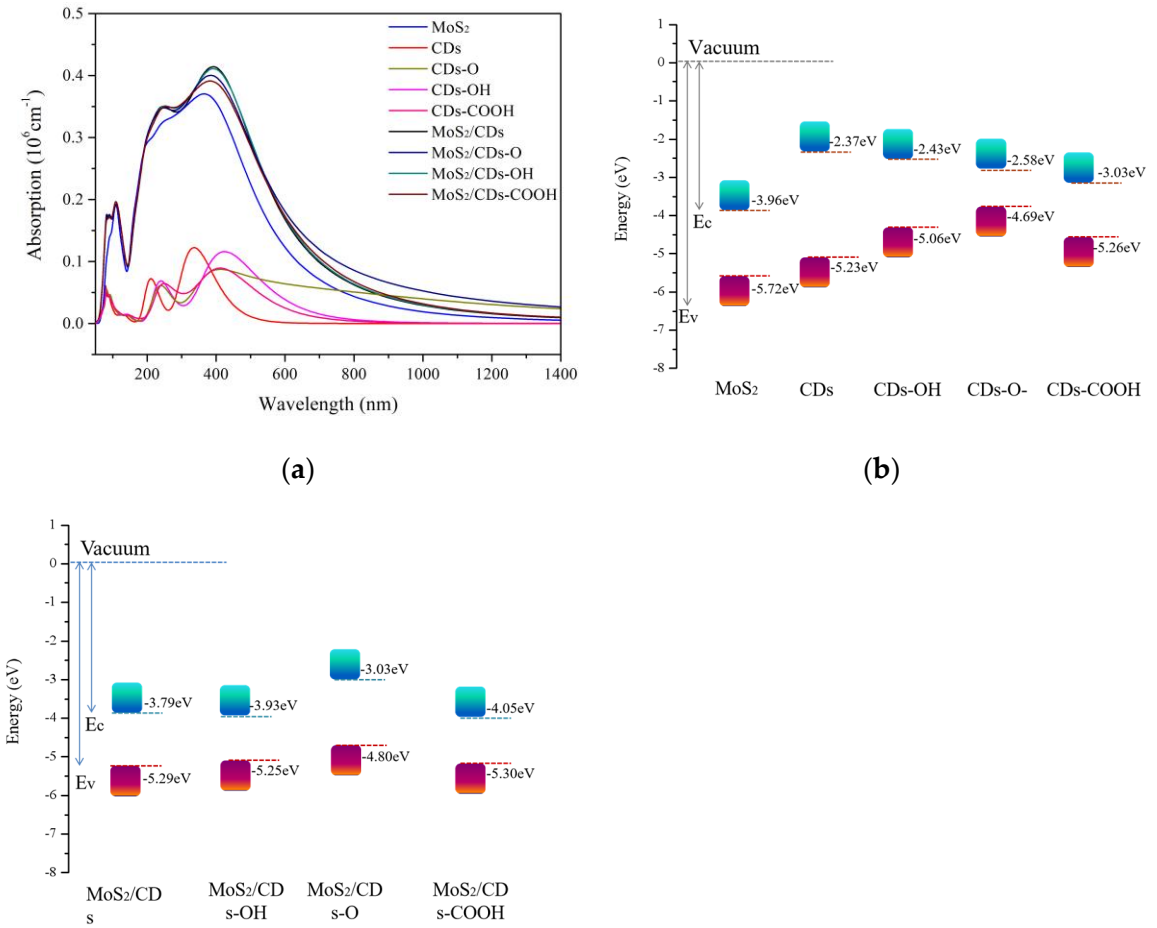

Figure 6. Optical absorption spectra (**a**); the calculated valence band maximum (VBM) and conduction band minimum (CBM) of MoS_2, CDs, CDs-OH, CDs-O, and CDs-COOH; (**b**) and MoS_2/CDs-T (**c**).

4. Conclusions

In summary, the impacts of hydroxyl, carbonyl, and carboxyl of the CDs on the structural, electronic, and optical properties of MoS_2/CDs were studied by employing density function theory. The more negative binding energies (−0.36 eV to −1.17 eV) between MoS_2 and CDs-T suggest that the hydroxyl, carbonyl, and carboxyl groups contribute to spontaneous combination and the stability structure. The three groups show opposite effects on the band gap of MoS_2/CDs-T. The hydroxyl and carboxyl greatly reduce the band gap (1.32 and 1.25 eV, respectively) compared with the band gap of MoS_2 and MoS_2/CDs. However, the carbonyl group slightly increases the band gap (1.77 eV). The heterostructure of MoS_2/CDs-T belongs to typical type-II band alignment, which is beneficial to the separation of photo-induced charge and hole. Notably, the carbonyl and carboxyl groups of CDs reduce the absorption intensity of MoS_2/CDs. In the preparation of MoS_2/CDs, the generation of carbonyl and carboxyl groups should be avoided as much as possible. Increasing the content of hydroxyl groups in carbon quantum dots is more conducive to improving the photocatalytic performance.

Author Contributions: Conceptualization, X.Y. and A.T.; methodology X.Y.; software, P.Y., A.T., X.Y., D.Z. and J.Y.; validation, Z.C., X.Y. and A.T.; formal analysis, P.Y., D.Z., J.Y., X.Y. and A.T.; investigation, X.Y. and A.T.; data curation, A.T.; writing—original draft preparation, X.Y. and A.T.; writing—review and editing, Z.C.; visualization, Z.C. and D.Z.; supervision, J.Y.; project administration, X.Y. and A.T.; funding acquisition, P.Y. All authors have read and agreed to the published version of the manuscript.

Funding: This research was funded by High Level Talents Funding Project of Hebei: Postdoctoral Research Project-Preferential Funding: B2020003021; Hebei Natural Science Foundation for Young Scientists: E2021202169. The APC was funded by Ansteel Beijing Research Institute Co., Ltd.

Data Availability Statement: Data are contained within the article.

Acknowledgments: Ansteel Beijing Research Institute Co., Ltd.; Pangang Group Vanadium Titanium & Resources Co., Ltd.; High Level Talents Funding Project of Hebei: Postdoctoral Research Project-Preferential Funding (B2020003021), and Hebei Natural Science Foundation for Young Scientists (E2021202169).

Conflicts of Interest: The authors declare no conflict of interest.

References

1. Singh, E.; Singh, P.; Kim, K.S.; Yeom, G.Y.; Nalwa, H.S. Flexible Molybdenum Disulfide (MoS_2) Atomic Layers for Wearable Electronics and Optoelectronics. *ACS Appl. Mater. Interfaces* **2019**, *11*, 11061–11105. [CrossRef] [PubMed]
2. Yuan, J.; Wang, F.; Patel, S.; Hu, Z.-L.; Tang, M.; Lou, J. Minimizing the Water Effect in Synthesis of High-Quality Monolayer MoS2 Nanosheets: Implications for Electronic and Optoelectronic Devices. *ACS Appl. Nano Mater.* **2021**, *4*, 8094–8100. [CrossRef]
3. Tang, K.; Qi, W.; Li, Y.; Wang, T. Electronic properties of van der Waals heterostructure of black phosphorus and MoS_2. *J. Phys. Chem. C* **2018**, *122*, 7027–7032. [CrossRef]
4. Morales-Guio, C.; Hu, X. Amorphous Molybdenum Sulfides as Hydrogen Evolution Catalysts. *Acc. Chem. Res.* **2014**, *47*, 2671–2681. [CrossRef]
5. Huang, Y.; Sun, Y.; Zheng, X.; Aoki, T.; Pattengale, B.; Huang, J.; He, X.; Bian, W.; Younan, S.; Williams, N.; et al. Atomically engineering activation sites onto metallic 1T-MoS2 catalysts for enhanced electrochemical hydrogen evolution. *Nat. Commun.* **2019**, *10*, 982. [CrossRef]
6. Lau, T.H.M.; Lu, X.; Kulhavý, J.; Wu, S.; Lu, L.; Wu, T.-S.; Kato, R.; Foord, J.S.; Soo, Y.-L.; Suenaga, K.; et al. Transition metal atom doping of the basal plane of MoS_2 monolayer nanosheets for electrochemical hydrogen evolution. *Chem. Sci.* **2018**, *9*, 4769–4776. [CrossRef]
7. Qin, W.; Chen, T.; Pan, L.; Niu, L.; Hu, B.; Li, D.; Li, J.; Sun, Z. MoS2-reduced graphene oxide composites via microwave assisted synthesis for sodium ion battery anode with improved capacity and cycling performance. *Electrochim. Acta* **2015**, *153*, 55–61. [CrossRef]
8. Zhou, Q.; Li, W.; Gao, M.; Xu, H.; Guo, Y.; Sun, L.; Zheng, D.; Lin, J. A truncated octahedron metal-organic framework derived TiO2@C@MoS2 composite with superior lithium-ion storage properties. *J. Power Sources* **2021**, *518*, 230746. [CrossRef]
9. Poudel, M.B.; Karki, H.P.; Kim, H.J. Silver nanoparticles decorated molybdenum sulfide/tungstate oxide nanorods as high performance supercapacitor electrode. *J. Energy Storage* **2020**, *32*, 101693. [CrossRef]
10. Jaramillo, T.F.; Jørgensen, K.P.; Bonde, J.; Nelsen, J.H.; Horch, S.; Chorkendorff, I. Identification of Active Edge Sites for Electrochemical H_2 Evolution from MoS_2 Nanocatalysts. *Science* **2007**, *317*, 100–102. [CrossRef]
11. Ganatra, R.; Zhang, Q. Few-Layer MoS_2: A Promising Layered Semiconductor. *ACS Nano* **2014**, *8*, 4074–4099. [CrossRef] [PubMed]
12. Zhang, X.; Huangfu, L.; Gu, Z.; Xiao, S.; Zhou, J.; Nan, H.; Gu, X.; Ostrikov, K. Controllable Epitaxial Growth of Large-Area MoS_2/WS_2 Vertical Heterostructures by Confined-Space Chemical Vapor Deposition. *Small* **2021**, *17*, 2007312. [CrossRef] [PubMed]
13. Zafiropoulou, I.; Katsiotis, M.S.; Boukos, N.; Karakassides, M.A.; Stephen, S.; Tzitzios, V.; Fardis, M.; Vladea, R.V.; Alhassan, S.M.; Papavassiliou, G. In Situ Deposition and Characterization of MoS2 Nanolayers on Carbon Nanofibers and Nanotubes. *J. Phys. Chem. C* **2013**, *117*, 10135–10142. [CrossRef]
14. Jing, Y.; Ortiz-Quiles, E.O.; Cabrera, C.R.; Chen, Z.; Zhou, Z. Layer-by-Layer Hybrids of MoS2 and Reduced Graphene Oxide for Lithium Ion Batteries. *Electrochim. Acta* **2014**, *147*, 392–400. [CrossRef]
15. Yin, Z.; Zhang, X.; Cai, Y.; Chen, J.; Wong, J.I.; Tay, Y.-Y.; Chai, J.; Wu, J.; Zeng, Z.; Zheng, B.; et al. Preparation of MoS_2-MoO_3Hybrid Nanomaterials for Light-Emitting Diodes. *Angew. Chem. Int. Ed.* **2014**, *53*, 12560–12565. [CrossRef]
16. Sahatiya, P.; Jones, S.S.; Badhulika, S. 2D MoS2–carbon quantum dot hybrid based large area, flexible UV–vis–NIR photodetector on paper substrate. *Appl. Mater. Today* **2018**, *10*, 106–114. [CrossRef]
17. Thangasamy, P.; Partheeban, T.; Sudanthiramoorthy, S.; Sathish, M. Enhanced Superhydrophobic Performance of BN-MoS2 Heterostructure Prepared via a Rapid, One-Pot Supercritical Fluid Processing. *Langmuir* **2017**, *33*, 6159–6166. [CrossRef]
18. Zhao, Y.-F.; Yang, Z.-Y.; Zhang, Y.-X.; Jing, L.; Guo, X.; Ke, Z.; Hu, P.; Wang, G.; Yan, Y.-M.; Sun, K.-N. Cu2O Decorated with Cocatalyst MoS2 for Solar Hydrogen Production with Enhanced Efficiency under Visible Light. *J. Phys. Chem. C* **2014**, *118*, 14238–14245. [CrossRef]
19. Ramakrishnan, S.; Karuppannan, M.; Vinothkannan, M.; Ramachandran, K.; Kwon, O.J.; Yoo, D.J. Ultrafine Pt Nanoparticles Stabilized by MoS_2/N-Doped Reduced Graphene Oxide as a Durable Electrocatalyst for Alcohol Oxidation and Oxygen Reduction Reactions. *ACS Appl. Mater. Interfaces* **2019**, *11*, 12504–12515. [CrossRef]
20. Poudel, M.B.; Ojha, G.P.; A Kim, A.; Kim, H.J. Manganese-doped tungsten disulfide microcones as binder-free electrode for high performance asymmetric supercapacitor. *J. Energy Storage* **2021**, *47*, 103674. [CrossRef]

21. Guo, J.; Zhu, H.; Sun, Y.; Tang, L.; Zhang, X. Doping MoS2 with Graphene Quantum Dots: Structural and Electrical Engineering towards Enhanced Electrochemical Hydrogen Evolution. *Electrochim. Acta* **2016**, *211*, 603–610. [CrossRef]
22. Heng, Z.W.; Chong, W.C.; Pang, Y.L.; Koo, C.H. An overview of the recent advances of carbon quantum dots/metal oxides in the application of heterogeneous photocatalysis in photodegradation of pollutants towards visible-light and solar energy ex-ploitation. *J. Environ. Chem. Eng.* **2021**, *9*, 105199. [CrossRef]
23. Chen, W.; Li, D.; Tian, L.; Xiang, W.; Wang, T.; Hu, W.; Hu, Y.; Chen, S.; Chen, J.; Dai, Z. Synthesis of graphene quantum dots from natural polymer starch for cell imaging. *Green Chem.* **2018**, *20*, 4438–4442. [CrossRef]
24. Luo, Z.; Qi, G.; Chen, K.; Zou, M.; Yuwen, L.; Zhang, X.; Huang, W.; Wang, L. Microwave-Assisted Preparation of White Fluorescent Graphene Quantum Dots as a Novel Phosphor for Enhanced White-Light-Emitting Diodes. *Adv. Funct. Mater.* **2016**, *26*, 2739–2744. [CrossRef]
25. Guo, X.; Wang, C.-F.; Yu, Z.-Y.; Chen, L.; Chen, S. Facile access to versatile fluorescent carbon dots toward light-emitting diodes. *Chem. Commun.* **2012**, *48*, 2692–2694. [CrossRef]
26. Su, W.; Wang, Y.; Wu, W.; Qin, H.; Song, K.; Huang, X.; Zhang, L.; Chen, D. Towards full-colour tunable photoluminescence of monolayer MoS2/carbon quantum dot ultra-thin films. *J. Mater. Chem. C* **2017**, *5*, 6352–6358. [CrossRef]
27. Gan, Z.; Wu, X.; Hao, Y. The mechanism of blue photoluminescence from carbon nanodots. *CrystEngComm* **2014**, *16*, 4981–4986. [CrossRef]
28. Zuo, P.; Lu, X.; Sun, Z.; Guo, Y.; He, H. A review on syntheses, properties, characterization and bioanalytical applications of fluorescent carbon dots. *Mikrochim. Acta* **2015**, *183*, 519–542. [CrossRef]
29. Sevilla, M.; Fuertes, A.B. Chemical and Structural Properties of Carbonaceous Products Obtained by Hydrothermal Carbonization of Saccharides. *Chem. Eur. J.* **2009**, *15*, 4195–4203. [CrossRef]
30. Poudel, M.B.; Awasthi, G.P.; Kim, H.J. Novel insight into the adsorption of Cr(VI) and Pb(II) ions by MOF derived Co-Al layered double hydroxide @hematite nanorods on 3D porous carbon nanofiber network. *Chem. Eng. J.* **2021**, *417*, 129312. [CrossRef]
31. Poudel, M.B.; Kim, H.J. Confinement of Zn-Mg-Al-layered double hydroxide and α-Fe_2O_3 nanorods on hollow porous carbon nanofibers: A free-standing electrode for solid-state symmetric supercapacitors. *Chem. Eng. J.* **2021**, *429*, 132345. [CrossRef]
32. Yan, J.-A.; Chou, M.-Y. Oxidation functional groups on graphene: Structural and electronic properties. *Phys. Rev. B* **2010**, *82*, 125403. [CrossRef]
33. Tang, S.; Wu, W.; Zhang, S.; Ye, D.; Zhong, P.; Li, X.; Liu, L.; Li, Y.-F. Tuning the activity of the inert MoS2 surface via graphene oxide support doping towards chemical functionalization and hydrogen evolution: A density functional study. *Phys. Chem. Chem. Phys.* **2018**, *20*, 1861–1871. [CrossRef] [PubMed]
34. Li, N.; Liu, Z.; Hu, S.; Chang, Q.; Xue, C.; Wang, H. Electronic and photocatalytic properties of modified MoS2/graphene quantum dots heterostructures: A computational study. *Appl. Surf. Sci.* **2019**, *473*, 70–76. [CrossRef]
35. Danovich, M.; Aleiner, I.L.; Drummond, N.D.; Fal'Ko, V. Fast Relaxation of Photo-Excited Carriers in 2-D Transition Metal Dichalcogenides. *IEEE J. Sel. Top. Quantum Electron.* **2016**, *23*, 168–172. [CrossRef]
36. Segall, M.D.; Lindan, P.J.D.; Probert, M.J.; Pickard, C.J.; Hasnip, P.J.; Clark, S.J.; Payne, M.C. First-principles simulation: Ideas, illustrations and the CASTEP code. *J. Phys. Condens. Matter* **2002**, *14*, 2717–2744. [CrossRef]
37. Perdew, J.P.; Burke, K.; Ernzerhof, M. Generalized gradient approximation made simple. *Phys. Rev. Lett.* **1996**, *77*, 3865. [CrossRef]
38. Su, J.; Feng, L.-P.; Zheng, X.; Hu, C.; Lu, H.; Liu, Z. Promising Approach for High-Performance MoS2 Nanodevice: Doping the BN Buffer Layer to Eliminate the Schottky Barriers. *ACS Appl. Mater. Interfaces* **2017**, *9*, 40940–40948. [CrossRef]
39. Zhang, J.; Lang, X.Y.; Zhu, Y.F.; Jiang, Q. Strain tuned InSe/MoS2 bilayer van der Waals heterostructures for photovoltaics or photocatalysis. *Phys. Chem. Chem. Phys.* **2018**, *20*, 17574–17582. [CrossRef]
40. Kośmider, K.; Fernández-Rossier, J. Electronic properties of the MoS_2-WS_2heterojunction. *Phys. Rev. B* **2013**, *87*, 075451. [CrossRef]
41. Li, Y.; Shu, H.; Wang, S.; Wang, J. Electronic and Optical Properties of Graphene Quantum Dots: The Role of Many-Body Effects. *J. Phys. Chem. C* **2015**, *119*, 4983–4989. [CrossRef]
42. Petkov, V.; Billinge, S.J.L.; Larson, P.; Mahanti, S.D.; Vogt, T.; Rangan, K.K.; Kanatzidis, M.G. Structure of nanocrystalline materials using atomic pair distribution function analysis: Study of $LiMoS_2$. *Phys. Rev. B* **2002**, *65*, 092105. [CrossRef]
43. Lauritsen, J.; Kibsgaard, J.; Helveg, S.; Topsøe, H.; Clausen, B.S.; Laegsgaard, E.; Besenbacher, F. Size-dependent structure of MoS_2 nanocrystals. *Nat. Nanotechnol.* **2007**, *2*, 53–58. [CrossRef]
44. Splendiani, A.; Sun, L.; Zhang, Y.; Li, T.; Kim, J.; Chim, C.-Y.; Galli, G.; Wang, F. Emerging photoluminescence in monolayer MoS_2. *Nano Lett.* **2010**, *10*, 1271–1275. [CrossRef]
45. Lee, H.S.; Min, S.-W.; Chang, Y.-G.; Park, M.K.; Nam, T.; Kim, H.; Kim, J.H.; Ryu, S.; Im, S. MoS_2 Nanosheet Phototransistors with Thickness-Modulated Optical Energy Gap. *Nano Lett.* **2012**, *12*, 3695–3700. [CrossRef]
46. Feng, L.-P.; Sun, H.-Q.; Li, A.; Su, J.; Zhang, Y.; Liu, Z.-T. Influence of Mo-vacancy concentration on the structural, electronic and optical properties of monolayer MoS_2: A first-principles study. *Mater. Chem. Phys.* **2018**, *209*, 146–151. [CrossRef]
47. Ong, W.-J.; Putri, L.K.; Tan, Y.-C.; Tan, L.-L.; Li, N.; Ng, Y.H.; Wen, X.; Chai, S.-P. Unravelling charge carrier dynamics in protonated g-C3N4 interfaced with carbon nanodots as co-catalysts toward enhanced photocatalytic CO2 reduction: A combined experimental and first-principles DFT study. *Nano Res.* **2017**, *10*, 1673–1696. [CrossRef]
48. Dürr, H. *Handbook of Photochemistry*; CRC Press: Boca Raton, FL, USA, 1994.
49. Gajdoš, M.; Hummer, K.; Kresse, G.; Furthmüller, J.; Bechstedt, F. Linear optical properties in the projector-augmented wave methodology. *Phys. Rev. B* **2006**, *73*, 045112. [CrossRef]

50. Shi, H.; Pan, H.; Zhang, Y.-W.; Yakobson, B.I. Quasiparticle band structures and optical properties of strained monolayer MoS_2 and WS_2. *Phys. Rev. B* **2013**, *87*, 155304. [CrossRef]
51. Kumar, A.; Ahluwalia, P. Ahluwalia, A first principle comparative study of electronic and optical properties of 1H-MoS_2 and 2H-MoS_2. *Mater. Chem. Phys.* **2012**, *135*, 755–761. [CrossRef]
52. Liang, W.Y.; A Wilson, J.; Yoffe, A.D. Optical studies of metal-semiconductor transmutations produced by intercalation. *J. Phys. C: Solid State Phys.* **1971**, *4*, L18–L20. [CrossRef]
53. Feng, L.-P.; Su, J.; Liu, Z.-T. Effect of vacancies on structural, electronic and optical properties of monolayer MoS_2: A first-principles study. *J. Alloys Compd.* **2014**, *613*, 122–127. [CrossRef]
54. Yang, C.-L.; Wang, M.-S.; Ma, X.G. First-principles study on the electronic and optical properties of WS_2 and MoS_2 monolayers. *Chin. J. Phys.* **2017**, *55*, 1930–1937. [CrossRef]
55. Li, Y.; Li, Y.-L.; Araujo, C.M.; Luo, W.; Ahuja, R. Single-layer MoS2 as an efficient photocatalyst. *Catal. Sci. Technol.* **2013**, *3*, 2214–2220. [CrossRef]